Noachian and more recent phyllosilicates in impact craters on Mars

Alberto G. Fairén[a,b,1], Vincent Chevrier[c], Oleg Abramov[d], Giuseppe A. Marzo[e,b], Patricia Gavin[c], Alfonso F. Davila[a,b], Livio L. Tornabene[f], Janice L. Bishop[a,b], Ted L. Roush[b], Christoph Gross[g], Thomas Kneissl[g], Esther R. Uceda[b], James M. Dohm[h], Dirk Schulze-Makuch[i], J. Alexis P. Rodríguez[j], Ricardo Amils[k], and Christopher P. McKay[b]

[a]Carl Sagan Center for the Study of Life in the Universe, 515 North Whisman Road, Mountain View, CA 94043; [b]Space Science and Astrobiology Division, National Aeronautics and Space Administration Ames Research Center, Moffett Field, CA 94035; [c]W. M. Keck Laboratory for Space and Planetary Simulation, Arkansas Space Center, University of Arkansas, Fayetteville, AR 72701; [d]Department of Geological Sciences, University of Colorado, Boulder, CO 80309; [e]Bay Area Environmental Research Institute, 560 Third Street West, Sonoma, CA 95476; [f]Lunar and Planetary Laboratory, University of Arizona, Tucson, AZ 85721; [g]Institute for Geological Sciences, Planetary Sciences and Remote Sensing, Freie Universität Berlin, Malteserstrasse 74-100, 12249 Berlin, Germany; [h]Department of Hydrology and Water Resources, University of Arizona, Tucson, AZ 85721; [i]School of Earth and Environmental Sciences, Washington State University, Pullman, WA 99164; [j]Planetary Science Institute, 1700E Fort Lowell, Tucson, AZ 85719; and [k]Centro de Astrobiología, 28850-Torrejón de Ardoz, Madrid, Spain

Edited by Norman H. Sleep, Stanford University, Stanford, CA, and approved May 10, 2010 (received for review March 4, 2010)

Hundreds of impact craters on Mars contain diverse phyllosilicates, interpreted as excavation products of preexisting subsurface deposits following impact and crater formation. This has been used to argue that the conditions conducive to phyllosilicate synthesis, which require the presence of abundant and long-lasting liquid water, were only met early in the history of the planet, during the Noachian period (>3.6 Gy ago), and that aqueous environments were widespread then. Here we test this hypothesis by examining the excavation process of hydrated minerals by impact events on Mars and analyzing the stability of phyllosilicates against the impact-induced thermal shock. To do so, we first compare the infrared spectra of thermally altered phyllosilicates with those of hydrated minerals known to occur in craters on Mars and then analyze the postshock temperatures reached during impact crater excavation. Our results show that phyllosilicates can resist the postshock temperatures almost everywhere in the crater, except under particular conditions in a central area in and near the point of impact. We conclude that most phyllosilicates detected inside impact craters on Mars are consistent with excavated preexisting sediments, supporting the hypothesis of a primeval and long-lasting global aqueous environment. When our analyses are applied to specific impact craters on Mars, we are able to identify both pre- and postimpact phyllosilicates, therefore extending the time of local phyllosilicate synthesis to post-Noachian times.

hydrothermal activity | impact cratering | Martian clays

Visible-infrared spectrometers orbiting Mars have identified multiple classes of hydrous minerals related to past aqueous activity (1–3). Phyllosilicates are particularly abundant and continue to be identified by OMEGA (Observatoire pour la Minéralogie, L'Eau, les Glaces et l'Activité, onboard Mars Express) (1) and CRISM (Compact Reconnaissance Imaging Spectrometer for Mars, onboard the Mars Reconnaissance Orbiter) (2). Phyllosilicates are indicative of the interaction of liquid water with rocks on or near the surface and have been identified in outcrops and scarps, such as depressions (3) and valleys (1), and in association with hundreds of impact craters in the southern highlands (2). These relationships have been interpreted to indicate that phyllosilicates are very old, early Noachian deposits (1, 3) formed in a time when the global environment on Mars was characterized by the presence of significant amounts of surface liquid water at very cold temperatures (4, 5). These phyllosilicate deposits were later buried by more recent materials and then exposed locally by impacts, faulting, or erosion.

We test this hypothesis here by analyzing the thermodynamically irreversible effects of the impact process, with an emphasis on the postshock heating and the extent of dehydration, dehydroxylation, and decomposition of preexisting hydrated minerals in the preimpact target. Our objective is to determine whether the occurrences and spatial distribution of phyllosilicate-rich materials within impact craters are consistent with their stability against thermal shock decomposition or if an alternative hypothesis considering postimpact synthesis should be invoked. We also describe the unique conditions occurring in specific locations within craters that may lead to the formation of phyllosilicates following the impact event, as well as discuss the appropriate methodologies to identify them using remotely acquired datasets. This postimpact alteration hypothesis has not yet received attention, but may be significant in the context of the potential occurrence of liquid water later in the history of Mars. Our results serve as an assessment of the magnitude and duration of the ancient Martian aqueous environments through validation of the impact exhumation hypothesis. We conclude our work with an in-depth analysis of a model impact event, the phyllosilicate-rich Toro crater.

Results

The Thermal Stability of Phyllosilicates. Hydrated/hydroxylated silicate minerals are characterized by a low thermal stability due to the presence of volatile components in their lattice, mainly bound H_2O and OH^- groups. Several studies have investigated the dehydroxylation process in Al and Fe phyllosilicates (e.g., refs. 6–8) and have concluded that dehydration in mixed-layer phyllosilicates starts at temperatures of ~100 °C (9, 10), implying modification in their near-infrared (NIR) spectra (8). We have experimentally tested the thermal stability of phyllosilicates against the shock-induced temperature increase created by an impact event (see *Materials and Methods*). We obtained laboratory spectra of heated samples of nontronite, montmorillonite, chlorite, kaolinite, prehnite, and serpentine (Fig. 1), all reported to be present on Mars (2, 3). We found that, at temperatures over 600 °C, phyllosilicates become unstable, resulting in phase transformation and loss of volatile components. The effects of such thermal alteration are remarkable in the IR spectra of the phyllosilicates, which show a decrease in intensity and broadening of the hydroxyl and hydration bands (1.4 and 1.9 μm) and flattening above the metal-OH absorption region (2.17–2.35 μm). Dehydroxylation was monitored through changes in the structural OH bands observed at 1.38–1.43 and 2.17–2.35 μm (11) for the phyllosilicates

Author contributions: A.G.F. designed research; A.G.F., V.C., O.A., G.A.M., P.G., C.G., and T.K. performed research; A.G.F., V.C., G.A.M., A.F.D., L.L.T., J.L.B., T.L.R., E.R.U., J.M.D., D.S.-M., A.P.R., R.A., and C.P.M. analyzed data; and A.G.F. wrote the paper.

The authors declare no conflict of interest.

This article is a PNAS Direct Submission.

[1]To whom correspondence should be addressed. E-mail: alberto.g.fairen@nasa.gov.

This article contains supporting information online at www.pnas.org/lookup/suppl/doi:10.1073/pnas.1002889107/-/DCSupplemental.

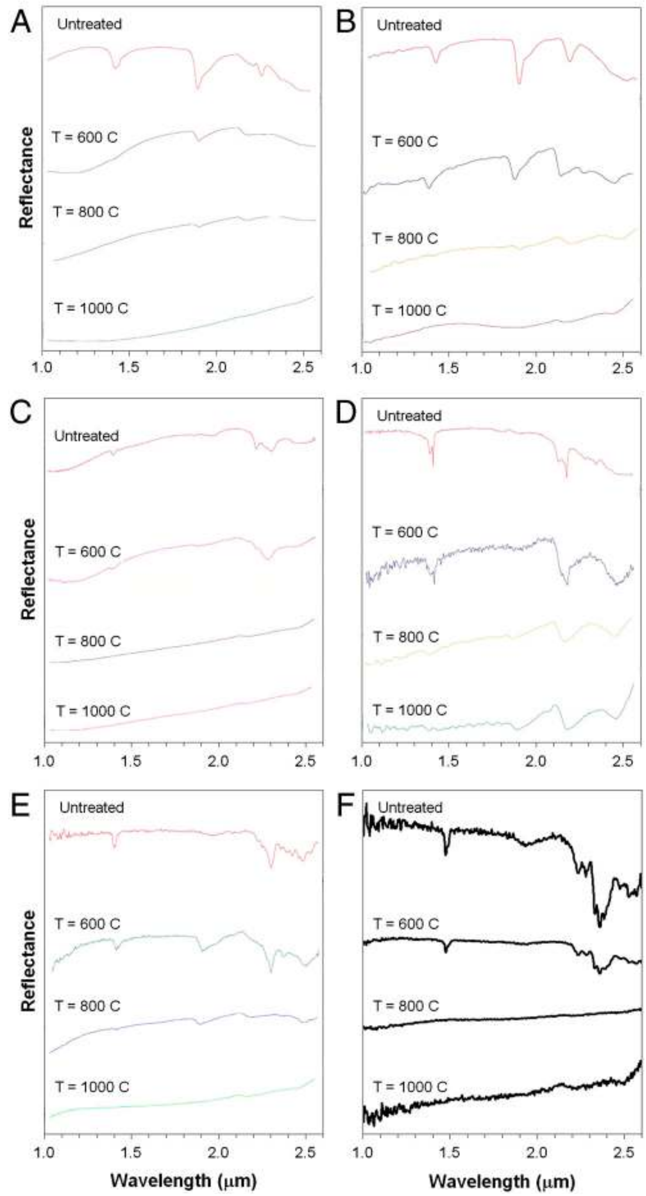

Fig. 1. Thermal stability of phyllosilicates. Laboratory reflectance spectral measurements illustrating the thermal stability of (*A*) nontronite, (*B*) montmorillonite, (*C*) chlorite, (*D*) kaolinite, (*E*) serpentine, and (*F*) prehnite.

analyzed here. Thermal transformations, and especially dehydroxylation, occur at or close to equilibrium. At temperatures above 800 °C, a severe modification of the characteristic spectral signatures is noted in the IR spectra of all phyllosilicates studied, which are altered into amorphous Fe-Mg-Al-rich silica glasses.

In contrast to OH^-, bound and adsorbed H_2O and the corresponding absorption band at 1.91 μm is observed only in smectites (nontronite and montmorillonite) (9, 11), but not in chlorite, prehnite, kaolinite, and serpentine. The adsorbed water molecules contribute to the shoulders near 1.46 and 1.97 μm and are largely removed after heating to relatively low temperatures (~150 °C), while the bound water is resistant up to higher temperatures and contributes to the bands at 1.41 and 1.91 μm (11, 12). The features near 1.9 μm in the spectra of heated smectites are likely due to water readsorbed by the samples during cooling, as when samples were not exposed to room air before measurements the 1.9-μm bands disappeared. Also, following sufficient heating to irreversibly disrupt the mineral structure, this band near 1.9 μm is no longer observed.

Postimpact Temperature Distributions. In the case of the impact excavation scenario, the majority of the highly shocked materials are dispersed in the crater fill, ejecta (proximal and distal) and deposited in subcrater floor injection dikes. Preexisting phyllosilicate deposits must survive the high temperatures reached during and after the impact event. High postshock temperatures are the result of the transfer of most of the kinetic energy of the impactor to the target and its transformation into heat (13, 14). As a consequence, preexisting surface and subsurface phyllosilicate-rich deposits may be subjected to very high temperatures that could alter hydrated and hydroxylated phases, especially where melt is in contact with the central peak of complex craters. Postimpact temperature distributions can be generated analytically with a good degree of accuracy (15).

We have calculated the maximum temperature increase in transient craters as a result of the impact (see *Materials and Methods*). Table 1 shows these values for three selected impactor sizes and for Mars-relevant impact velocities and target parameters. We have also calculated the radius of the areas heated to temperatures above 600 and 800 °C, which we have found to cause significant modifications in the IR spectra of the phyllosilicates. In general, for a given crater diameter, higher impact velocities result in higher temperatures, and the presence of water ice in the subsurface lowers the temperatures due to the latent heat of melting and vaporization of water (14, 15). Our results show that temperatures inside the crater during the impact event do not reach values over those observed in the laboratory for the thermal stability of phyllosilicates, except in a central area around the point of impact. The radius of this area is dependent upon the size and composition of the projectile and the presence of ice in the target material and can represent up to 30% of the crater radius for larger craters (>100 km diameter).

Discussion

When comparing our laboratory results of thermal stability of phyllosilicates and modeled postimpact temperature distributions on Mars, we show that preexisting phyllosilicate sediments will largely remain unaffected by the meteoritic and/or cometary impact, as long as they are located outside of the maximum shock-temperature region generated during the impact. Our results have two immediate consequences. First, as a general rule, we demonstrate that phyllosilicates in Martian crater floors, walls, rims, and ejecta blankets have not been subject to postshock temperatures high enough to alter their spectral features and, therefore, can be excavated preexisting sediments. This supports the hypothesis that the widespread occurrence of phyllosilicates inside impact craters is informative of a primeval planetary global hydrological system, characterized by the presence of lasting bodies of liquid water in which clays precipitated (1). And second, as an exception to the general rule, our results imply that those hydrated minerals situated in the central areas of the craters were substantially affected by high temperatures during impact excavation, and their infrared spectra ought to show evidence of this thermal alteration. Further, postshock temperatures are at their maximum in the central area of the crater and can be sufficiently high and long-lasting to support a hydrothermal system and induce the formation of new hydrated/hydroxylated phases or the alteration of existing ones (see *SI Text*). Therefore, phyllosilicates found in central areas of impact craters are likely to have formed after the impact event.

But it is important to point out that the phyllosilicates identified in the central area of impact craters can also be preexisting phyllosilicate sediments. In general, low-shock rocks of the central structural uplift originate from just below the highly shocked, melt-lined transient crater floor and are subsequently exposed by uplift through these materials (14). These rocks are generally subjected to lower shock effects, and the dominant consequences are brecciation and fracturing with minimal to no amorphization

Table 1. Maximum temperature increases in the transient crater as a result of asteroid (density = 3,000 kg/m^3) impacts on Mars

$D_r = 50$ km		$D_p = 3.8$ km $D_{tr} = 34$ km	$D_p = 3.0$ km $D_{tr} = 34$ km
	Dry	$\Delta T_{max} = 490\,°C$ $D_{>600\,C} = 0$ km $D_{>800\,C} = 0$ km	$\Delta T_{max} = 710\,°C$ $D_{>600\,C} = 11$ km $D_{>800\,C} = 0$ km
	Wet	$\Delta T_{max} = 278\,°C$ $D_{>600\,C} = 0$ km $D_{>800\,C} = 0$ km	$\Delta T_{max} = 512\,°C$ $D_{>600\,C} = 0$ km $D_{>800\,C} = 0$ km
$D_r = 100$ km		$D_p = 8.4$ km $D_{tr} = 63$ km	$D_p = 6.7$ km $D_{tr} = 63$ km
	Dry	$\Delta T_{max} = 970\,°C$ $D_{>600\,C} = 26$ km $D_{>800\,C} = 18$ km	$\Delta T_{max} = 1100\,°C$ $D_{>600\,C} = 36$ km $D_{>800\,C} = 30$ km
	Wet	$\Delta T_{max} = 789\,°C$ $D_{>600\,C} = 18$ km $D_{>800\,C} = 0$ km	$\Delta T_{max} = 1100\,°C$ $D_{>600\,C} = 30$ km $D_{>800\,C} = 22$ km
$D_r = 150$ km		$D_p = 13.3$ km $D_{tr} = 90$ km	$D_p = 10.6$ km $D_{tr} = 90$ km
	Dry	$\Delta T_{max} = 1100\,°C$ $D_{>600\,C} = 48$ km $D_{>800\,C} = 39$ km	$\Delta T_{max} = 1300\,°C$ $D_{>600\,C} = 60$ km $D_{>800\,C} = 52$ km
	Wet	$\Delta T_{max} = 1100\,°C$ $D_{>600\,C} = 39$ km $D_{>800\,C} = 32$ km	$\Delta T_{max} = 1140\,°C$ $D_{>600\,C} = 52$ km $D_{>800\,C} = 46$ km

Maximum temperatures in the final crater depend on the surface temperature and geothermal gradient at the impact site, but are typically within 0–20%. D_r, rim-ro-rim final crater diameter; D_p, diameter of the projectile; D_{tr}, rim-ro-rim transient crater diameter; Dry, dry basalt target; Wet, wet basalt target (20% ice by volume); ΔT_{max}, maximum temperature increase in the transient crater; $D_{>600\,C}$, diameter within the transient crater where the ΔT is higher than 600 °C; $D_{>800\,C}$, diameter within the transient crater where the ΔT is higher than 800 °C.

or melting. Hence they remain relatively coherent and unaltered through the crater formation process. Any postshock hydrothermal alteration on these rocks will be restricted to areas along fractures and will not be pervasive throughout the entire outcrop in the uplift. Preexisting phyllosilicates could be brought to the surface inside these rocks and ultimately be exposed in the central crater uplift.

This geologic complexity of the impact process, together with our limited accessibility to Martian craters, makes it necessary to define strategies to distinguish between preexisting phyllosilicate-rich materials and newly synthesized hydrated phases in central crater uplifts through remote sensing datasets. Here we propose two different approaches. First, the formation environment may be very different between the two hypothesized scenarios listed above, as high temperatures may not be required in the preimpact formation, but will certainly exist following the impact event. Therefore, identification of lower temperature mineral phases will undoubtedly point to preexisting materials. On the contrary, identification of higher temperature mineral phases may allow both interpretations of postimpact hydrothermal alteration or excavation of preexisting hydrothermal products, as it has been proposed that Noachian phyllosilicates on Mars were formed as a direct effect of impact gardening (16). Second, if the phyllosilicate signatures are observed to be largely associated with excavated megablocks and clasts, then this will suggest that they originated as preexisting target materials. On the other hand, if hydrated minerals appear to be genetically independent from megabreccia, and chiefly associated with factures, ridges, or morphologic features indicative of a postimpact alteration environment, then they are likely to be hydrothermally produced after the impact excavation. The alternative that phyllosilicates are brought to the surface inside megablocks and then eroded, distributed by winds, and finally imprinted over areas not associated with megablocks cannot be discarded, but is less likely.

In the end, a more conclusive identification of preexisting phyllosilicate-bearing materials can be made with a higher degree of certainty, while characterization of postimpact minerals is far more challenging. High-resolution spectral and spatial data are necessary to make the best possible assessment between preexisting excavated phyllosilicates and postimpact hydrothermal minerals in the central area of each particular impact crater. The postimpact hydrothermal alteration can readily explain the synthesis of phyllosilicates after the Noachian period, and it is appropriate for describing the key facts that allow such a process to be recognized.

Toro Crater: A Case Study

We present here a detailed study of the phyllosilicate deposits that we have identified within one particular impact crater, that we named Toro (International Astronomical Union approval on November 24, 2008). The selected crater is located on the northern margin of the Syrtis Major volcanic province, centered near 71.8E, 17.0N (Fig. 2*A*). Toro is a complex crater 42 km in diameter and 2 km in depth (Fig. 2*B*). The central structural uplift of Toro resulted in the formation of a central peak and associated pit. The central peak complex (both peak and central pit) is approximately 8 km in diameter with its highest peaks rising more than 300 m above the crater floor. Abundant and diverse phyllosilicate signatures have been observed through analysis of CRISM images in the greater Nili Fossae region (17), including Toro crater (18). Here we focus on the identification of distinct hydrated silicate deposits inside Toro using CRISM NIR hyperspectral images (see *Materials and Methods*). Toro exhibits a distinct occurrence of material consistent with extensive hydrated and hydroxylated silicate deposits (17, 18), which includes smec-

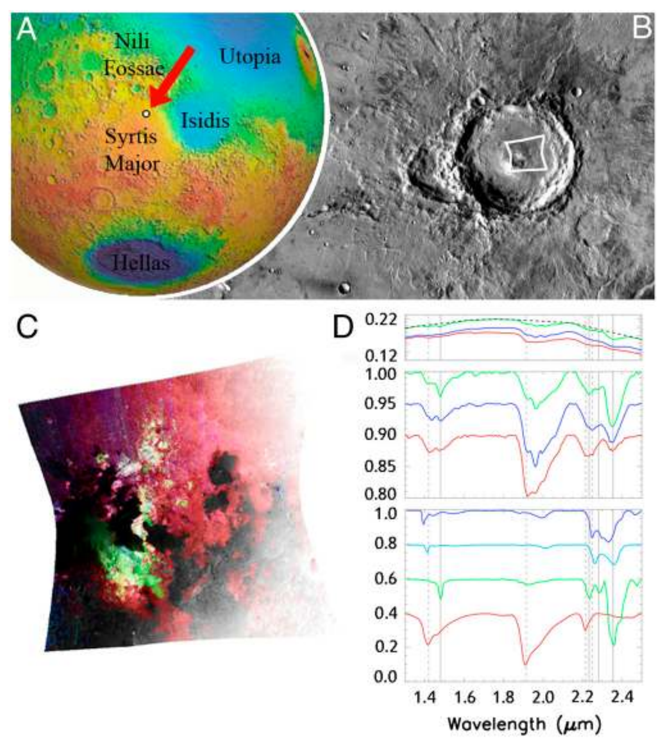

Fig. 2. Physiographic and geochemical setting of Toro crater. (*A*) MOLA colorized shaded relief map of Mars centered on Toro (red arrow). (*B*) THEMIS grayscale mosaic of Toro. The hourglass shape represents the location of the CRISM observation shown in *C*. (*C*) CRISM observation FRT0000B1B5 in false colors: red, smectites; green, prehnite; blue, chlorites. Yellow and magenta are mixed hydrated phases. (*D Top*) CRISM I/F corrected for the geometry of the observation and the atmosphere. The thick dashed line represents an example of the function used to remove the continuum. The results of the continuum removal are shown in the *Middle*. (*Bottom*) Some continuum removed laboratory reflectance spectra. The green spectrum is compared to RELAB spectrum C1ZE03 of prehnite. The blue spectra are compared to a 50% mixture of clinochlore (dark blue) and chamosite (light blue) (9). The red spectrum is compared to CRIMS Spectral Library spectrum 397F174 of smectite.

GEOLOGY

tites, prehnite, chlorite, and hydrated amorphous silica or opaline material (Fig. 2 *C* and *D*). Smectites are pervasively spread throughout the northern part of the crater wall and partially covering the crater floor, especially within the northern part of the impact crater basin, a distribution compatible with excavated preimpact materials (Fig. 2*c* and Fig. S1).

To search for possible postimpact phyllosilicates in Toro, we have (*i*) calculated the specific shock-induced ΔT underneath the transient Toro crater and (*ii*) analyzed the mineral distribution of higher temperature phyllosilicates in the central uplift of the crater. Crater counting indicates that Toro has an estimated age of 3.62 ± 0.1 Ga (Fig. S2) and therefore is Hesperian in age. We assume for the Hesperian Period a mean surface temperature around −75 °C (19) and a geothermal heat flow gradient of 50 °C/km, four times higher (19) than at present (20, 21). Fig. 3 shows the cases for different asteroid diameters and different vertical impact velocities, calibrated to give the correct final crater size. Our model results show that the impacted preexisting materials, which now form the central uplift, reached a minimum T near 650 to 800 °C (depending on input variables) during the excavation of Toro. Therefore, only those phyllosilicates included inside excavated megablocks could have survived impact temperatures in the area where the central uplift emerges now.

The spatial relationships between crater morphology and hydrated phase signatures can be substantiated at the CRISM and HiRISE (High Resolution Imaging Science Experiment) resolutions: Prehnite is observed to have an evident genetic association with a distinct high-standing peak located within the central uplift complex, hereafter referred to as the "southern peak" (Fig. 4). The southern peak shows a massive texture associated with some breccia fragments and impact-melt deposits, with no layered outcrops (Fig. 4*B*) (18), suggesting that it was severely modified subsequent to impact excavation. The alteration possibly included amorphization or melting conducing to the hydrothermal synthesis of prehnite. Another peak located on the north side of the central uplift, hereafter referred to as "northern peak," displays a megablock with intact stratigraphy surrounded and unconformably overlain by megabreccia deposits

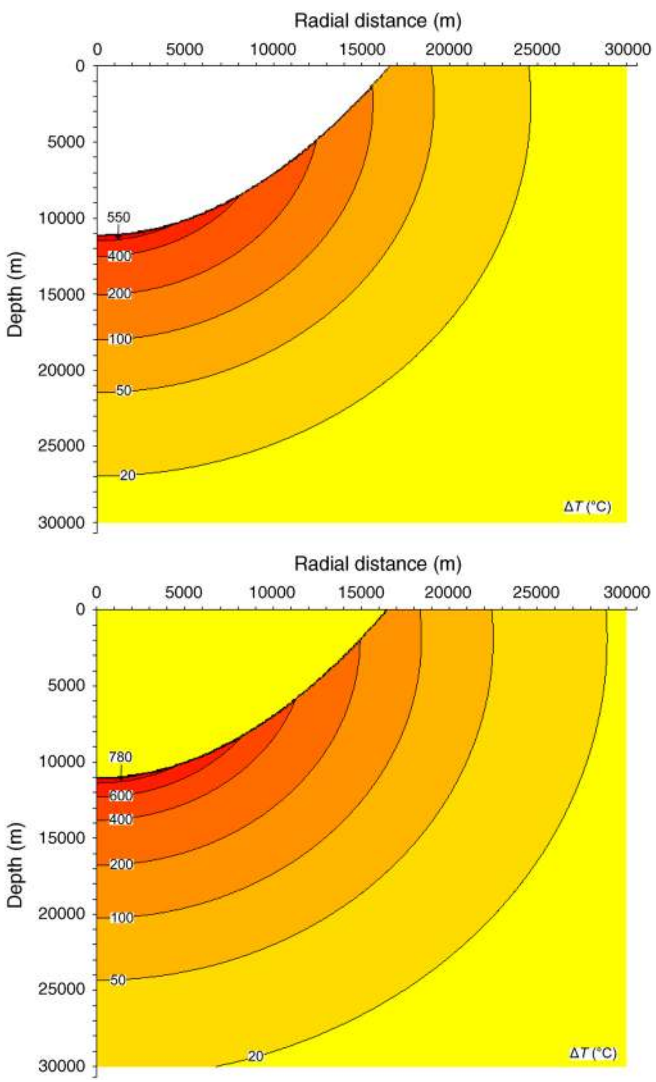

Fig. 3. Central temperatures in the transient Toro crater. (*A*) A 3.1-km asteroid with a density of 3,000 kg/m^3 impacting vertically at 8 km/s. (*B*) A 2.5-km asteroid at 12 km/s. Higher sizes and/or velocities will yield higher temperatures (see Table 1). Asteroid diameters and impact velocities were chosen to keep the crater diameter constant.

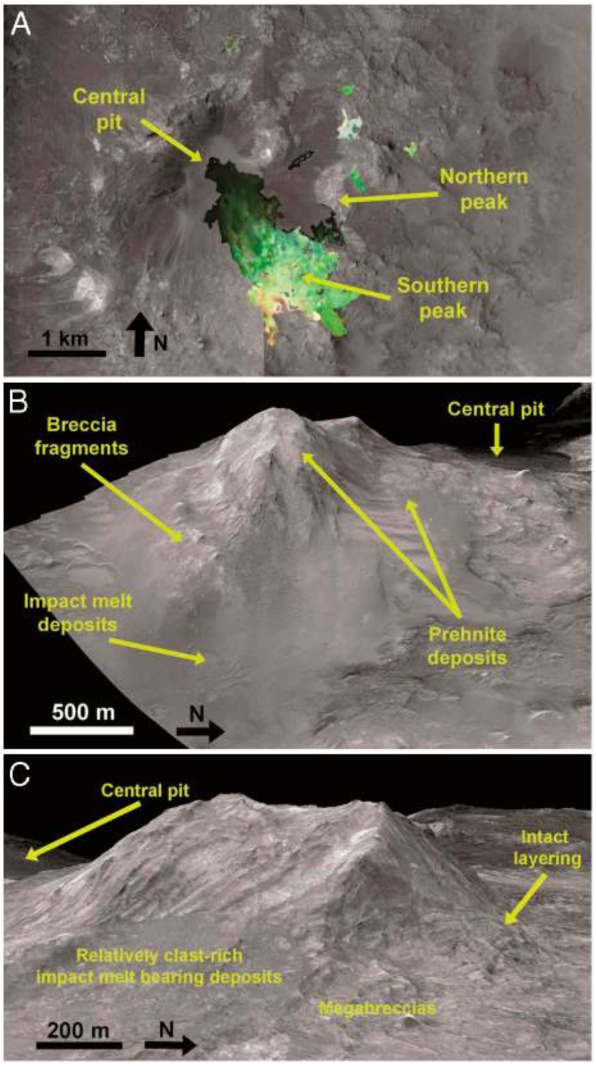

Fig. 4. Distribution of prehnite inside Toro crater. (*A*) Portions of HiRISE images PSP_005842_1970, PSP_009270_1970, and ESP_011538_1970 covering Toro's central uplift complex and surrounding crater floor. CRISM observation FRT0000B1B5 is highlighted in green to indicate the presence of prehnite. The peaks described in *B* and *C* are labeled. (*B*) Digital elevation model of the southern peak. Prehnite seems to be shed from the top of the peak and scattered to the northwest into the central pit. (*C*) Digital elevation model of the northern peak, showing intact light- and dark-toned layers and fractured and brecciated bedrock. Models derived using SOCET set v5.4.1 (BAE systems) on the PSP_005842_1970 and ESP_011538_1970 stereo pair (NASA/JPL/ASU) at a scale of 2 m per post and a vertical exaggeration of 5×.

(Fig. 4*C*). This megablock represents intact preexisting target stratigraphy that was excavated and uplifted by the Toro-forming event. The northern peak lacks prehnite, strongly suggesting that prehnite was not forming part of the preimpact sediments. In addition, the CRISM prehnite spectrum of the southern peak shows a prominent 2.35-μm absorption band (Fig. 2*D*). Based upon our laboratory experiments (Fig. 1*F*), this is consistent with unheated or slightly heated prehnite (<600 °C), in contrast with the minimum calculated postimpact temperatures for the central uplift of Toro (>650 °C). Finally, in a relative sense, prehnite is a higher-temperature phyllosilicate and has been reported to form hydrothermally at elevated temperatures (22, 23). These facts are informative of prehnite exposures in Toro formed as the result of postimpact hydrothermal activity during the Hesperian.

The mineral distributions and geological relationships described here for Toro crater appear in many craters (see *SI Text* and Fig. S3) and so are not rare or uncommon on the surface of Mars. Strategies toward confirming a hydrothermal origin for the phyllosilicates in the central uplifts of Martian impact craters merit continued attention for planning future missions to Mars, as they will shed light on the possibility of post-Noachian synthesis of phyllosilicates, extending the time for precipitation of hydrated minerals further to more recent times than what has been assumed to date. In addition, the implied aqueous activity would provide direct evidence that these environments possessed habitable conditions in terms of energy and liquid water availability (24) during post-Noachian times.

Conclusions

We have combined remote sensing analyses, laboratory investigations, and theoretical models to address questions about the origin of phyllosilicates in and around Martian craters, providing an experimental basis for the characterization of the formation processes of phyllosilicates in impact craters on Mars. We assess the effects of highly shock-heated materials via impact-related excavation and modification in order to understand the nature of phyllosilicates. We have demonstrated that preexisting phyllosilicate sediments can survive the impact exhumation temperatures if they are located outside of the peak shock area during the impact process. This means that phyllosilicates reported in crater floors, walls, rims, and ejecta are consistent with excavated preexisting deposits. The widespread presence of phyllosilicates associated with craters in the southern highlands suggests that the primeval Martian sediments have an important phyllosilicate component. These ancient deposits provide information about an initial geological period on Mars characterized by the presence of widespread aqueous environments with a geochemistry conducive to the global synthesis of phyllosilicate minerals. Detailed analyses may also reveal the local presence of phyllosilicates precipitated in hydrothermal systems in and around the point of impact and triggered by the impact event, suggesting that such altered materials could be produced in any time period in which a large crater is excavated. Only by means of high resolution data is it possible to begin to differentiate between the two genetic mechanisms, pre- vs. postimpact formation of phyllosilicates in central uplifts. We have used this methodology to show that some phyllosilicates associated with Toro crater were formed by impact-triggered hydrothermalism after the Noachian.

Materials and Methods

Thermal Analyses of Phyllosilicates. Experiments were carried out by placing 1-g samples of each phyllosilicate in the center of a ceramic heating tube and then in a Lindberg high-temperature tube oven. The samples were heated to temperatures ranging from ~300 to ~1100 °C for durations from 4 to 24 h in air as well as under a steady flow of CO_2 to more closely simulate the early Martian atmosphere. The ovens required about 1 h to reach the selected temperature for each experiment. After the samples were heated, the ovens were allowed to cool overnight, and the samples were removed and weighed. Detailed experimental details are also given elsewhere (25, 26).

Postimpact Temperature Distributions. Shock-deposited heat is calculated using the Murnaghan equation of state for specific waste heat (27). To obtain the final temperature increase, specific waste heat is divided by the heat capacity of the target rock. We have tested impact velocities of 8 and 12 km/s, as the average asteroid impact velocity for Mars is 9.3 km/s (28). We have modeled 90° impacts to estimate the maximum values of the temperatures in the center of the crater. For oblique impacts, temperatures will be lower, and therefore the radius of the area where phyllosilicates cannot survive will be smaller. Complete model details are given in *SI Text*.

CRISM Data Acquisition for Toro. CRISM spatial resolution is 18–20 m/pixel, with a spectral resolution of 6.55 μm/channel in the range 362–3920 μm (29). NIR spectra are selected for the identification of phyllosilicates, from 1.3 to 2.5 μm. CRISM data have been converted to apparent I/F (the ratio of reflected to incident sunlight), then divided by the cosine of the incidence angle to correct for the illumination geometry (29, 30). The gas atmospheric contribution has been removed using an improved volcano-scan technique correction (31), which considers two spectral bands at 1.980 μm and 2.007 μm instead of the usual 1.890 μm and 2.011 μm (29, 32). This choice retains the rapid analyses capabilities of the previous volcano-scan techniques and provides for more thorough analyses of surface hydration. Once distinct CRISM end members have been identified, we removed a straight line continuum to isolate the spectral features. Based upon the positions of spectral features observed, we are able to associate regions inside and outside every crater with specific types of minerals.

ACKNOWLEDGMENTS. E. Pierazzo provided a critical review that helped improve the original manuscript. We thank the MRO CRISM and HiRISE teams for collecting the data used in this study.

GEOLOGY

1. Bibring JP, et al. (2006) Global mineralogical and aqueous Mars history derived from OMEGA/Mars Express data. *Science* 312:400–404.
2. Mustard JF, et al. (2008) Hydrated silicate minerals on Mars observed by the Mars Reconnaissance Orbiter CRISM instrument. *Nature* 454:305–309.
3. Murchie SL, et al. (2009) A synthesis of Martian aqueous mineralogy after one Mars year of observations from the Mars Reconnaissance Orbiter. *J Geophys Res* 114:E00D06 doi:10.1029/2009JE003342.
4. Fairén AG, et al. (2009) Stability against freezing of aqueous solutions on early Mars. *Nature* 459:401–404.
5. Fairén AG (2010) A cold and wet Mars. *Icarus* 208:165–175.
6. Brindley GW, Lemaitre J (1987) *Chemistry of Clays and Clay Minerals*, ed ACD Newman (Longman, London), pp 319–370.
7. Frost RL, Ruan H, Kloprogge JT, Gates WP (2000) Dehydration and dehydroxylation of notronites and ferruginous smectite. *Thermochim Acta* 346:63–72.
8. Milliken RE, Mustard JF (2005) Quantifying absolute water content of minerals using near-infrared reflectance spectroscopy. *J Geophys Res* 110:E12001 doi:10.1029/2005JE002534.
9. Bishop JL, Pieters CM, Edwards JO (1994) Infrared spectroscopic analyses on the nature of water in montmorillonite. *Clay Clay Miner* 42:701–715.
10. Byrappa K, Yoshimura M (2001) *Handbook of Hydrothermal Technology*, eds GE McGuire, SM Rossnagel, and RF Bunshah (Noyes Publications/William Andrew Publishing, Park Ridge, NJ/Norwich, NY).
11. Bishop JL, Lane MD, Dyar MD, Brown AJ (2008) Reflectance and emission spectroscopy study of four groups of phyllosilicates: Smectites, kaolinite-serpentines, chlorites and micas. *Clay Miner* 43:35–54.
12. Farmer VC, Russell JD (1971) Interlayer complexes in layer silicates. The structure of water in lamellar ionic solutions. *T Faraday Soc* 67:2737–2749.
13. Melosh HJ (1989) *Impact Cratering: A Geologic Process* (Oxford Univ Press, New York).
14. French BM (1998) *Traces of Catastrophe: A Handbook of Shock-Metamorphic Effects in Terrestrial Meteorite Impact Structures* (Lunar and Planetary Inst, Houston), p 120.
15. Abramov O, Mojzsis SJ (2009) Microbial habitability of the Hadean Earth during the late heavy bombardment. *Nature* 459:419–422.
16. Schwenzer SP, Kring DA (2009) Impact-generated hydrothermal systems capable of forming phyllosilicates on Noachian Mars. *Geology* 37:1091–1094.
17. Ehlmann BL, et al. (2009) Identification of hydrated silicate minerals on Mars using MRO-CRISM: Geologic context near Nili Fossae and implications for aqueous alteration. *J Geophys Res* 114:E00D08 doi:10.1029/2009JE003339.
18. Marzo GA, et al. (2010) Evidence for Hesperian impact-induced hydrothermalism on Mars. *Icarus* doi:10.1016/j.icarus.2010.03.013.
19. Kargel J, et al. (2007) Martian hydrogeology sustained by thermally insulating gas and salt hydrates. *Geology* 35:975–978.
20. Clifford SM (1993) A model for the hydrologic and climatic behaviour of water of Mars. *J Geophys Res* 98:10973–11016.
21. Prieto-Ballesteros O, et al. (2006) Interglacial clathrate destabilization in Mars: Possible contributing source of its atmospheric methane. *Geology* 34:149–152.

22. Liou JG (1971) Synthesis and stability relations of prehnite, $Ca_2Al_2Si_3O_{10}(OH)_2$. *Am Mineral* 56:507–531.
23. Hall AJ, Banks D, Fallick AE, Hamilton PJ (1989) An hydrothermal origin for copper-impregnated prehnite and analcime from Boylestone Quarry, Barrhead, Scotland. *J Geol Soc* 146:701–713.
24. Cockell CS, Lee P (2002) The biology of impact craters—a review. *Biol Rev* 77:279–310.
25. Gavin P, Chevrier V (2010) Thermal alteration of nontronite and montmorillonite: Implications for the martian surface. *Icarus* doi:10.1016/j.icarus.2010.02.027.
26. Ostrowski D, Gietzen K, Lacy CS, Sears DWG (2010) An investigation of the presence and nature of phyllosilicates on the surface of C asteroids by an analysis of the continuum slopes in their near infrared region. *Meteor Planet Sci*, in press.
27. Kieffer SW, Simonds CH (1980) The role of volatiles and lithology in the impact cratering process. *Rev Geophys Space Phys* 18:143–181.
28. Steel D (1998) Distributions and moments of asteroid and comet impact speeds upon the Earth and Mars. *Planet Space Sci* 46:473–478.
29. Murchie SL, et al. (2007) Compact Reconnaissance Imaging Spectrometer for Mars (CRISM) on Mars Reconnaissance Orbiter (MRO). *J Geophys Res* 112:E05S03 doi:10.1029/2006JE002682.
30. Murchie SL, et al. (2009) Compact Reconnaissance Imaging Spectrometer for Mars investigation and data set from the Mars Reconnaissance Orbiter's primary science phase. *J Geophys Res* 114:E00D07 doi:10.1029/2009JE003344.
31. McGuire PC, et al. (2009) An improvement to the volcano-scan algorithm for atmospheric correction of CRISM and OMEGA spectral data. *Planet Space Sci* 57:809–815.
32. Erard S, Calvin W (1997) New composite spectra of Mars, 0.4–5.7 mum. *Icarus* 130:449–460.